

Projectile structure effects in the Coulomb breakup of one-neutron halo nuclei

Rajdeep Chatterjee ^{a,1}, Prabir Banerjee ^{a,2} and
Radhey Shyam ^{a,3}

^a*Theory Group, Saha Institute of Nuclear Physics, 1/AF Bidhan Nagar,
Calcutta - 700 064, INDIA.*

Abstract

We investigate the Coulomb breakup of neutron rich nuclei ^{11}Be and $^{19,17,15}\text{C}$ within a theory developed in the framework of Distorted Wave Born Approximation. Finite range effects are included by a local momentum approximation, which allows incorporation of realistic wave functions for these nuclei in our calculations. Energy and angular as well as parallel momentum distributions of the fragments emitted in the breakup of these nuclei on heavy targets have been calculated using several structure models for their ground state. Comparison with the available experimental data shows that the results are selective about the ground state wave function of the projectile. Our investigations confirm that the nuclei ^{11}Be , ^{19}C and ^{15}C have a one-neutron halo structure in their ground states. However, for ^{17}C such a structure appears to be less likely. Calculations performed within our method have also been compared with those from an adiabatic model and the results are discussed.

PACS numbers: 21.10.Hw, 21.60.-n, 24.10.Eq, 25.60.Gc

Key words: Coulomb breakup, one-neutron halo nucleus, effects of projectile structure.

1 Introduction

It has now been well established that close to the neutron drip line, there exist nuclei having one, or some times two, very loosely bound valence neutrons extending too far out in space with respect to a dense charged core [1]. The

¹ e-mail: raja@tnp.saha.ernet.in

² e-mail: prabir@tnp.saha.ernet.in

³ e-mail: shyam@tnp.saha.ernet.in

properties of these neutron halo nuclei [2] have been reviewed by several authors (see e.g. [3–6]). The halo systems, which involve a new form of nuclear matter, are characterized by large reaction and Coulomb dissociation cross sections [7–10]. Moreover, in the breakup reactions induced by these nuclei, the angular distributions of neutrons measured in coincidence with the core nuclei [11,12] are strongly forward peaked and the parallel momentum distributions of the core fragment have very narrow widths [13–18]. Due to their strikingly different properties as compared to those of the stable nuclei, such systems provide a stringent test of the nuclear structure models developed for the latter.

The Coulomb dissociation is a significant reaction channel in the scattering of halo nuclei from a stable heavy target nucleus. It provides a convenient tool to investigate their structure. For instance, it would place constraints on their electric dipole response [9,10,19,20]. Of course, in the Serber [21] type of models [22,23], the breakup cross sections are directly related to the momentum space wave function of the projectile ground state. The studies of the Coulomb dissociation of weakly bound nuclei are also of interest due to their application in determining the cross sections of the astrophysically interesting radiative capture reactions at solar temperatures [24].

The Coulomb dissociation of halo nuclei has been investigated by several authors recently, using a number of different theoretical approaches. A semiclassical coupled channel formalism has been used by authors of Ref. [25], while in Refs. [26,27] the relative motion of the core and the valence particle is described by a time dependent Schrödinger equation. The results within these approaches depend on the range of the impact parameter associated with the straight line trajectories used to describe the motion of the projectile in the field of target nuclei. However, in these studies the emphasis was on investigating the dynamics of the Coulomb dissociation, and not the structure of the projectile ground state which was assumed to have some very simple zero range (ZR) form. Similar assumption for the projectile structure was also made in other semiclassical [23,28] and prior form distorted wave Born approximation (DWBA) calculations [29].

On the other hand, the post form DWBA theory of the breakup reactions incorporates the details of the ground state structure of the projectile in the breakup amplitude [30]. However, in an earlier application [31] of this theory to calculate the breakup of the halo nuclei, the simplifying approximation of the zero range interaction was used. This approximation necessarily excludes the use of this theory to describe the breakup of non- s – wave projectiles. Moreover its applicability is questionable even for s – wave projectiles at higher beam energies [32]. Therefore, to investigate the details of the projectile structure through breakup reactions within this theory, the inclusion of the finite range effects is necessary. It may be noted that in a recently formulated adiabatic

model [33] of the Coulomb breakup reactions, where it is assumed that the projectile excitation is predominantly to the states of the low internal energy, the details of the ground state wave function also enters in the transition amplitude.

In this paper, we present a theoretical model to describe the Coulomb breakup of a projectile within the framework of the post form DWBA where finite range effects are included, approximately, via a local momentum approximation (LMA) [34,35]. The exact treatment of the finite range effects within this theory, although desirable, is much too complicated as it would lead to six dimensional integrals involving functions which are oscillatory asymptotically. The LMA leads to two simplifying features. First, it factorises the dynamics of the reaction from the structure effects of the projectile and second, it results in an amplitude where the term describing the dynamics of the process is the same as that evaluated in the ZR approximation. We present the application of this theory to the Coulomb breakup of neutron rich nuclei ^{11}Be and $^{15,17,19}\text{C}$ on a number of heavy targets. We attempt to put constraints on the ground state structure of these nuclei by analyzing almost all the available data on the energy, angular and longitudinal momentum distributions of fragments using various configurations of the projectile ground state.

Our formalism is presented in section 2. In section 3 we present and discuss the results of our calculations for various observable for the reactions mentioned above. The summary and the conclusions of our work are described in section 4. The validity of the approximate method used by us to include the finite range effects is presented in appendix A.

2 Formalism

We consider the reaction $a + t \rightarrow b + c + t$, where the projectile a breaks up into fragments b (charged) and c (uncharged) in the Coulomb field of a target t . The coordinate system chosen is shown in Fig. 1.

The position vectors satisfy the following relations

$$\mathbf{r} = \mathbf{r}_i - \alpha \mathbf{r}_1, \quad \alpha = \frac{m_c}{m_c + m_b} \quad (1)$$

$$\mathbf{r}_c = \gamma \mathbf{r}_1 + \delta \mathbf{r}_i, \quad \delta = \frac{m_t}{m_b + m_t}, \quad \gamma = (1 - \alpha\delta) \quad (2)$$

The exact post form T - matrix for this case is

$$T = \langle \chi_b^{(-)}(\mathbf{k}_b, \mathbf{r}) \Phi_b(\xi_b) \chi_c^{(-)}(\mathbf{k}_c, \mathbf{r}_c) \Phi_c(\xi_c) | V_{bc}(\mathbf{r}_1) | \Psi_a^{(+)}(\xi_a, \mathbf{r}_1, \mathbf{r}_i) \rangle, \quad (3)$$

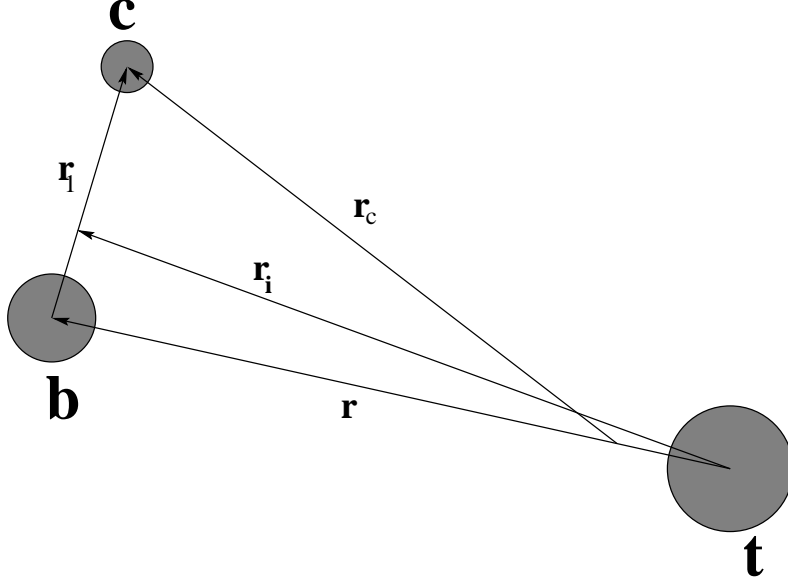


Fig. 1. The three-body coordinate system. b , c and t represent the charged core, valence neutron and target respectively.

where χ 's are the distorted waves for relative motions of b and c with respect to t and the center of mass (c.m.) of $b+t$ system respectively, and Φ 's are the internal state wave functions of the concerned particles with internal coordinates ξ . $\Psi_a^{(+)}(\xi_a, \mathbf{r}_1, \mathbf{r}_i)$ is the exact three-body scattering wave function of the projectile with a wave vector \mathbf{k}_a , with outgoing wave boundary condition. \mathbf{k}_b , \mathbf{k}_c are Jacobi wave vectors of b and c respectively in the final channel of the reaction. $V_{bc}(\mathbf{r}_1)$ is the interaction between b and c . The charged fragment b interacts with the target by a point Coulomb interaction and hence $\chi_b^{(-)}(\mathbf{k}_b, \mathbf{r})$ is a Coulomb distorted wave with incoming wave boundary condition. For pure Coulomb breakup, the interaction between the target and uncharged fragment c is zero and hence $\chi_c^{(-)}(\mathbf{k}_c, \mathbf{r}_c)$ is replaced by a plane wave.

In the distorted wave Born approximation (DWBA), we write

$$\Psi_a^{(+)}(\xi_a, \mathbf{r}_1, \mathbf{r}_i) = \Phi_a(\xi_a, \mathbf{r}_1)\chi_a^{(+)}(\mathbf{k}_a, \mathbf{r}_i), \quad (4)$$

where $\Phi_a(\xi_a, \mathbf{r}_1)$ represents the bound state wave function of the projectile having its radial and angular parts as $u_\ell(r_1)$ and $Y_{\ell m}(\hat{\mathbf{r}}_1)$ respectively, which are associated with the relative motion of b and c . $\chi_a^{(+)}(\mathbf{k}_a, \mathbf{r}_i)$ is the Coulomb distorted scattering wave describing the relative motion of the c.m. of the projectile with respect to the target with outgoing wave boundary condition. The assumption inherent in Eq. (4) is that the breakup channels are very weakly coupled and hence this coupling needs to be treated only in the first order. The transition amplitude (written in the integral form) is now given by

$$T = \int \int \int d\xi d\mathbf{r}_1 d\mathbf{r}_i \chi_b^{(-)*}(\mathbf{k}_b, \mathbf{r}) \Phi_b^*(\xi_b) e^{-i\mathbf{k}_c \cdot \mathbf{r}_c} \Phi_c^*(\xi_c) V_{bc}(\mathbf{r}_1) \times \Phi_a(\xi_a, \mathbf{r}_1) \chi_a^{(+)}(\mathbf{k}_a, \mathbf{r}_i). \quad (5)$$

The integrals over the internal coordinates ξ give

$$\int d\xi \Phi_b^*(\xi_b) \Phi_c^*(\xi_c) \Phi_a(\xi_a, \mathbf{r}_1) = \sum_{\ell m j \mu} \langle \ell m j_c \mu_c | j \mu \rangle \langle j_b \mu_b j \mu | j_a \mu_a \rangle i^\ell u_\ell(r_1) Y_{\ell m}(\hat{\mathbf{r}}_1). \quad (6)$$

In Eq. (6) ℓ is the relative motion angular momentum between b and c . This is coupled to spin of c and the resultant j is coupled to spin of (the inert core) b to get the spin of a (j_a). Using Eq. (6), the T -matrix can be written as

$$T = \sum_{\ell m j \mu} \langle \ell m j_c \mu_c | j \mu \rangle \langle j_b \mu_b j \mu | j_a \mu_a \rangle i^\ell \hat{\ell} \beta_{\ell m}(\mathbf{k}_b, \mathbf{k}_c; \mathbf{k}_a), \quad (7)$$

where

$$\hat{\ell} \beta_{\ell m}(\mathbf{k}_b, \mathbf{k}_c; \mathbf{k}_a) = \int \int d\mathbf{r}_1 d\mathbf{r}_i \chi_b^{(-)*}(\mathbf{k}_b, \mathbf{r}) e^{-i\mathbf{k}_c \cdot \mathbf{r}_c} V_{bc}(\mathbf{r}_1) \times \phi_a^{\ell m}(\mathbf{r}_1) \chi_a^{(+)}(\mathbf{k}_a, \mathbf{r}_i), \quad (8)$$

with $\beta_{\ell m}$ being the reduced T - matrix and $\hat{\ell} = \sqrt{2\ell + 1}$. We have written $\phi_a^{\ell m}(\mathbf{r}_1) = u_\ell(r_1) Y_{\ell m}(\hat{\mathbf{r}}_1)$.

It may be noted that the reduced amplitude $\beta_{\ell m}$ involves a six dimensional integral which makes its evaluation quite complicated. The problem gets further acute due to the fact that the integrand involves three scattering waves which have oscillatory behavior asymptotically. Therefore, several approximate methods have been used in the literature to avoid the evaluation of six dimensional integrals. In the zero range approximation (ZRA) [36] one assumes

$$V_{bc}(\mathbf{r}_1) \phi_a^{\ell m}(\mathbf{r}_1) = D_0 \delta(\mathbf{r}_1), \quad (9)$$

where D_0 is the usual zero range constant. This approximation reduces the six dimensional integral in Eq.(8) to a three-dimensional one. The corresponding amplitude is written as

$$\beta_{00}^{ZR} = D_0 \langle \chi_b^{(-)}(\mathbf{k}_b, \mathbf{r}_i) e^{i\delta \mathbf{k}_c \cdot \mathbf{r}_i} | \chi_a^{(+)}(\mathbf{k}_a, \mathbf{r}_i) \rangle. \quad (10)$$

In Eq. (10), the details of the projectile structure enter in the reaction amplitude only as a multiplicative constant D_0 . However, ZRA necessarily restricts

the relative motion between b and c in the projectile a to s – state only. Even for such cases, this approximation may not be satisfied for heavier projectiles and at higher beam energies [32].

Baur and Trautmann (BT) [37] have proposed an alternative approximate scheme in which the projectile c.m. coordinate in the corresponding distorted wave in Eq. (8) is replaced by that of the core-target system, i.e. $\mathbf{r}_i \approx \mathbf{r}$. With this approximation the amplitude $\beta_{\ell m}$ splits into two factors each involving a three dimensional integral

$$\hat{\ell}\beta_{\ell m}^{BT} = \langle e^{i\mathbf{k}_c \cdot \mathbf{r}_1} | V_{bc} | \phi_a^{\ell m}(\mathbf{r}_1) \rangle \langle \chi_b^{(-)}(\mathbf{k}_b, \mathbf{r}) e^{i\delta \mathbf{k}_c \cdot \mathbf{r}} | \chi_a^{(+)}(\mathbf{k}_a, \mathbf{r}) \rangle. \quad (11)$$

The first term, known as the form factor, depends on the structure of the projectile through its ground state wave function $\phi_a^{\ell m}(\mathbf{r}_1)$. The second term involves the dynamics of the reaction. This amplitude (which will be referred to as the BT amplitude), used originally to study the deuteron breakup at sub-Coulomb energies [37], was applied to the calculations of the Coulomb breakup of halo nuclei in [31]. This approximation, which allows the application of the theory to non- s – wave projectiles, may seem to be justified if the c.m. of the $b + c$ system is shifted towards b (which is indeed the case if $m_b \gg m_c$). However, the neglected piece of \mathbf{r}_i ($\alpha \mathbf{r}_1$) occurs in association with the wave vector \mathbf{k}_a , whose magnitude may not be negligible for the reactions at the higher beam energies. Therefore, contribution coming to the amplitude from the neglected part of \mathbf{r}_i may still be substantial.

An approximate way of taking into account the finite range effects in the post form DWBA theory is provided by the local momentum approximation [32,34]. The attractive feature of this approximation is that it leads to the factorization of the amplitude $\beta_{\ell m}$ similar to that obtained in the BT case. We use this approximation to write the Coulomb distorted wave of particle b in the final channel as

$$\chi_b^{(-)}(\mathbf{k}_b, \mathbf{r}) = e^{-i\alpha \mathbf{K} \cdot \mathbf{r}_1} \chi_b^{(-)}(\mathbf{k}_b, \mathbf{r}_i). \quad (12)$$

Eq. (12) represents an exact Taylor series expansion about \mathbf{r}_i if $\mathbf{K}(= -i\nabla_{\mathbf{r}_i})$ is treated exactly. However, this is not done in the LMA scheme. Instead, the magnitude of the local momentum here is taken to be

$$K(R) = \sqrt{\frac{2m}{\hbar^2}(E - V(R))}, \quad (13)$$

where m is the reduced mass of the $b - t$ system, E is the energy of particle b relative to the target in the c.m. system and $V(R)$ is the Coulomb potential between b and the target at a distance R . Therefore, the local momentum \mathbf{K} is

evaluated at some distance R , and its magnitude is held fixed for all the values of \mathbf{r} . As is discussed in appendix A, the results of our calculations are almost independent of the choice of the direction the local momentum. Therefore, we have taken the directions of \mathbf{K} and \mathbf{k}_b to be the same in all the calculations presented in this paper. It may be noted that in the calculations presented in Ref. [38], the LMA was applied to the Coulomb distorted wave of the projectile channel, where making a choice of the direction of the local momentum is somewhat complicated due to the fact that the directions of both the fragments in the final channel has to be brought into the consideration. Detailed discussion on the validity of the local momentum approximation is presented in appendix A.

Substituting Eq. (12) into Eq. (8) we get the following factorized form of the amplitude

$$\begin{aligned} \hat{\ell}\beta_{\ell m}^{FRDWBA} &= \langle e^{i(\gamma\mathbf{k}_c - \alpha\mathbf{K})\cdot\mathbf{r}_1} |V_{bc}| \phi_a^{\ell m}(\mathbf{r}_1) \rangle \\ &\times \langle \chi_b^{(-)}(\mathbf{k}_b, \mathbf{r}_i) e^{i\delta\mathbf{k}_c\cdot\mathbf{r}_i} | \chi_a^{(+)}(\mathbf{k}_a, \mathbf{r}_i) \rangle. \end{aligned} \quad (14)$$

Eq. (14) (which will be referred to as the FRDWBA amplitude in the following) looks like Eq (11) of the BT theory but with the very important difference that the form factor is now evaluated at the momentum transfer $(\gamma\mathbf{k}_c - \alpha\mathbf{K})$, and not at the valence particle momentum \mathbf{k}_c . The two momenta could be quite different for cases of interest in this paper. The second term, involving the dynamics part of the reaction, is the same in both the cases. Therefore, the breakup amplitude obtained in BT approximation differs from that of FRDWBA by a factor

$$F_r = \frac{\beta_{\ell m}^{BT}}{\beta_{\ell m}^{FRDWBA}} = \frac{\langle e^{i\mathbf{k}_c\cdot\mathbf{r}_1} |V_{bc}| \phi_a^{\ell m}(\mathbf{r}_1) \rangle}{\langle e^{i(\beta\mathbf{k}_c - \alpha\mathbf{K})\cdot\mathbf{r}_1} |V_{bc}| \phi_a^{\ell m}(\mathbf{r}_1) \rangle} \quad (15)$$

Recently, a theory of the Coulomb breakup has been developed within an adiabatic (AD) model [33,39], where one assumes that the excitation of the projectile is such that the relative energy (E_{bc}) of the $b - c$ system is much smaller than the total incident energy, which allows E_{bc} to be replaced by the constant separation energy of the fragments in the projectile ground state. It was shown in [39] that under these conditions the wave function $\Psi_a^{(+)}(\xi_a, \mathbf{r}_1, \mathbf{r}_i)$ has an exact solution as given below

$$\Psi_a^{(+),AD}(\xi_a, \mathbf{r}_1, \mathbf{r}_i) = \Phi_a(\xi_a, \mathbf{r}_1) e^{i\alpha\mathbf{k}_a\cdot\mathbf{r}_1} \chi_a^{(+)}(\mathbf{k}_a, \mathbf{r}) \quad (16)$$

Substituting $\Psi_a^{(+),AD}$ for $\Psi_a^{(+)}$ in Eq. (3) leads to the reduced amplitude:

$$\hat{\ell}\beta_{\ell m}^{AD} = \langle e^{i(\mathbf{k}_c - \alpha\mathbf{k}_a)\cdot\mathbf{r}_1} | V_{bc} | \phi_a^{\ell m}(\mathbf{r}_1) \rangle \langle \chi_b^{(-)}(\mathbf{k}_b, \mathbf{r}) e^{i\delta\mathbf{k}_c\cdot\mathbf{r}} | \chi_a^{(+)}(\mathbf{k}_a, \mathbf{r}) \rangle. \quad (17)$$

This amplitude differs from those of BT as well as FRDWBA only in the form factor part (first term), which is evaluated here at the momentum transfer $(\mathbf{k}_c - \alpha\mathbf{k}_a)$. Eq. (17) can also be obtained in the DWBA model by making a local momentum approximation to the Coulomb distorted wave in the initial channel of the reaction, and by evaluating the local momentum at $R = \infty$ with its direction being the same as that of the projectile [38]. The adiabatic model does not make the weak coupling approximation of the DWBA. However, it necessarily requires one of the fragments (in this case c) to be chargeless. In contrast, the DWBA with the LMA could, in principle, be applied to cases where both the fragments b and c are charged [32] (of course the dynamical part of the amplitude can not be expressed in terms of the simple bremsstrahlung integral in this case as discussed below). While the effect of nuclear breakup in the adiabatic model description of elastic scattering of the loosely bound projectile has been calculated in Ref. [39–41], the nuclear part of the amplitude for breakup reactions is yet to be calculated within this model. At the same time, the nuclear breakup cross section has not been calculated within the FRDWBA theory also (although it is straightforward to do so). These calculations will be presented in a future publication.

The triple differential cross section of the reaction is given by

$$\frac{d^3\sigma}{dE_b d\Omega_b d\Omega_c} = \frac{2\pi}{\hbar v_a} \rho(E_b, \Omega_b, \Omega_c) \sum_{\ell m} |\beta_{\ell m}|^2, \quad (18)$$

where $\rho(E_b, \Omega_b, \Omega_c)$ is the appropriate [42] three-body phase space factor, given by

$$\rho(E_b, \Omega_b, \Omega_c) = \frac{h^{-6} m_b m_c m_t p_b p_c}{m_t + m_c - m_c \frac{\mathbf{k}_c \cdot (\mathbf{k}_a - \mathbf{k}_b)}{k_c^2}}, \quad (19)$$

with \mathbf{k}_a , \mathbf{k}_b and \mathbf{k}_c being evaluated in the appropriate frame of reference. v_a is the relative velocity of the projectile in the initial channel. p in Eq. (19) are the linear momenta which are related to wave numbers k by $p = \hbar k$.

Substituting the following expressions for the Coulomb distorted waves

$$\chi_b^{(-)*}(\mathbf{k}_b, \mathbf{r}_i) = e^{-\pi\eta_b/2} \Gamma(1 + i\eta_b) e^{-i\mathbf{k}_b\cdot\mathbf{r}_i} {}_1F_1(-i\eta_b, 1, i(k_b r_i + \mathbf{k}_b\cdot\mathbf{r}_i)), \quad (20)$$

$$\chi_a^{(+)}(\mathbf{k}_a, \mathbf{r}_i) = e^{-\pi\eta_a/2} \Gamma(1 + i\eta_a) e^{i\mathbf{k}_a\cdot\mathbf{r}_i} {}_1F_1(-i\eta_a, 1, i(k_a r_i - \mathbf{k}_a\cdot\mathbf{r}_i)) \quad (21)$$

in Eq. (14), one gets for the triple differential cross section

$$\frac{d^3\sigma}{dE_b d\Omega_b d\Omega_c} = \frac{2\pi}{\hbar v_a} \rho(E_b, \Omega_b, \Omega_c) \frac{4\pi^2 \eta_a \eta_b}{(e^{2\pi\eta_b} - 1)(e^{2\pi\eta_a} - 1)} |I|^2 4\pi \sum_{\ell} |Z_{\ell}|^2. \quad (22)$$

In Eqs. (20 – 22) η 's are the Coulomb parameters for the concerned particles. In Eq. (22) I is the Bremsstrahlung integral [43] which can be evaluated in a closed form:

$$I = -i \left[B(0) \left(\frac{dD}{dx} \right)_{x=0} (-\eta_a \eta_b) {}_2F_1(1 - i\eta_a, 1 - i\eta_b; 2; D(0)) \right. \\ \left. + \left(\frac{dB}{dx} \right)_{x=0} {}_2F_1(-i\eta_a, -i\eta_b; 1; D(0)) \right] \quad (23)$$

where

$$B(x) = \frac{4\pi}{k^{2(i\eta_a + i\eta_b + 1)}} \left[(k^2 - 2\mathbf{k} \cdot \mathbf{k}_a - 2xk_a)^{i\eta_a} (k^2 - 2\mathbf{k} \cdot \mathbf{k}_b - 2xk_b)^{i\eta_b} \right], \quad (24)$$

$$D(x) = \frac{2k^2(k_a k_b + \mathbf{k}_a \cdot \mathbf{k}_b) - 4(\mathbf{k} \cdot \mathbf{k}_a + xk_a)(\mathbf{k} \cdot \mathbf{k}_b + xk_b)}{(k^2 - 2\mathbf{k} \cdot \mathbf{k}_a - 2xk_a)(k^2 - 2\mathbf{k} \cdot \mathbf{k}_b - 2xk_b)} \quad (25)$$

with $\mathbf{k} = \mathbf{k}_a - \mathbf{k}_b - \delta\mathbf{k}_c$. Z_{ℓ} contains the projectile structure information and is given by

$$Z_{\ell} = \int dr_1 r_1^2 j_{\ell}(k_1 r_1) V_{bc}(\mathbf{r}_1) u_{\ell}(r_1), \quad (26)$$

with $k_1 = |\gamma\mathbf{k}_c - \alpha\mathbf{K}|$.

3 Calculations and discussions

Apart from the distance at which local momentum is calculated (which is taken to be 10 *fm* as discussed in appendix A) and its direction (described already in the previous section), the only other input to our calculations is the radial part of the projectile ground state wave function. The forms for this as chosen by us for the projectiles considered in this paper are discussed in the following.

3.1 Calculations for reactions induced by ^{11}Be

For the ground state of ^{11}Be , we have considered the following configurations : (a) a *s* – wave valence neutron coupled to 0^+ ^{10}Be core ($^{10}\text{Be}(0^+) \otimes 1s_{1/2\nu}$)

with a one-neutron separation energy ($S_{n-^{10}\text{Be}}$) of 504 keV and a spectroscopic factor (SF) of 0.74 [44–46], (b) a d – wave valence neutron coupled to 2^+ ^{10}Be core ($^{10}\text{Be}(2^+) \otimes 0d_{5/2}\nu$) with a binding energy of 3.872 MeV (which is the sum of energy of the excited 2^+ core (3.368 MeV) and $S_{n-^{10}\text{Be}}$) and (c) an admixture of these two configurations with spectroscopic factors of 0.74 and 0.17 respectively [47]. In each case, the single particle wave function, is constructed by assuming the valence neutron- ^{10}Be interaction to be of Woods-Saxon type whose depth is adjusted to reproduce the corresponding value of the binding energy with fixed values of the radius and diffuseness parameters (taken to be 1.15 fm and 0.5 fm respectively). For configuration (a), this gives a potential depth of 71.03 MeV, a root mean square (rms) radius for the valence neutron of 6.7 fm and a rms radius for ^{11}Be of 2.91 fm when the size of the ^{10}Be core is taken to be 2.28 fm [48]. In some cases we have also used a wave function for the s – state of ^{11}Be calculated within a dynamical core polarization (DCP) model [49].

3.1.1 Energy distributions of the fragments

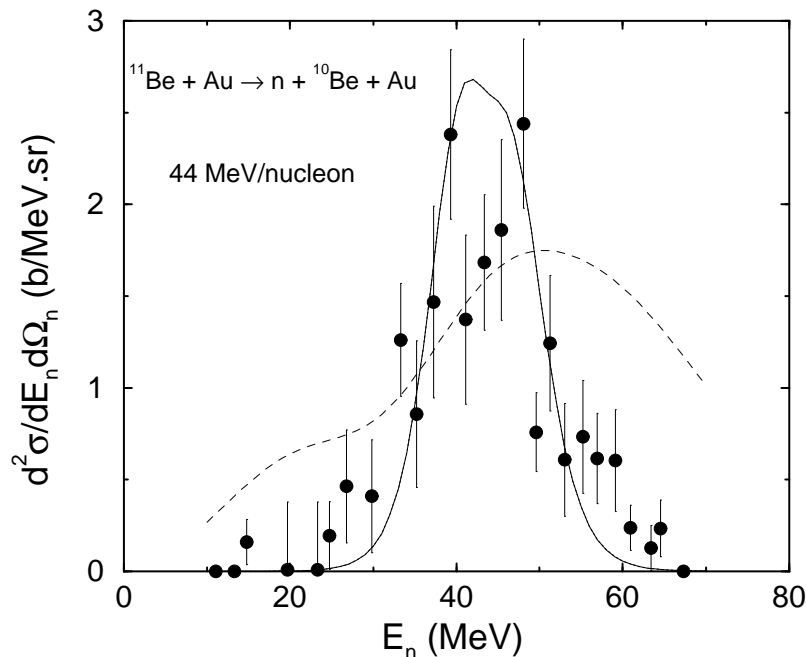


Fig. 2. Neutron energy distributions for the breakup of ^{11}Be on the Au target at the beam energy of 44 MeV/nucleon calculated within the FRDWBA using configurations (a) (dotted line), (b) (dashed line, plotted after multiplying the actual results by a factor of 1000) and (c) solid line for the ground state of ^{11}Be . The results obtained with configurations (a) and (c) are indistinguishable from each other. The experimental data are taken from [28].

In Fig. 2, we present the results of our FRDWBA calculations for the double differential cross section ($d^2\sigma/dE_n d\Omega_n$) as a function of the neutron energy

at the neutron angle of 1° , in the breakup of ^{11}Be on a gold target at the beam energy of 44 MeV/nucleon. The experimental data are taken from [28]. The results obtained with configurations (a), (b) and (c) for the ground state of ^{11}Be are shown by dotted, dashed and full lines respectively. The results of configuration (b) are plotted after multiplying the actual numbers by a factor of 1000. The cross sections obtained with configurations (a) and (c) are indistinguishable from each other. Thus these two configurations produce almost identical results for the Coulomb dissociation of ^{11}Be . In the following, we have used configuration (a) for the ground state state of ^{11}Be in all the calculations.

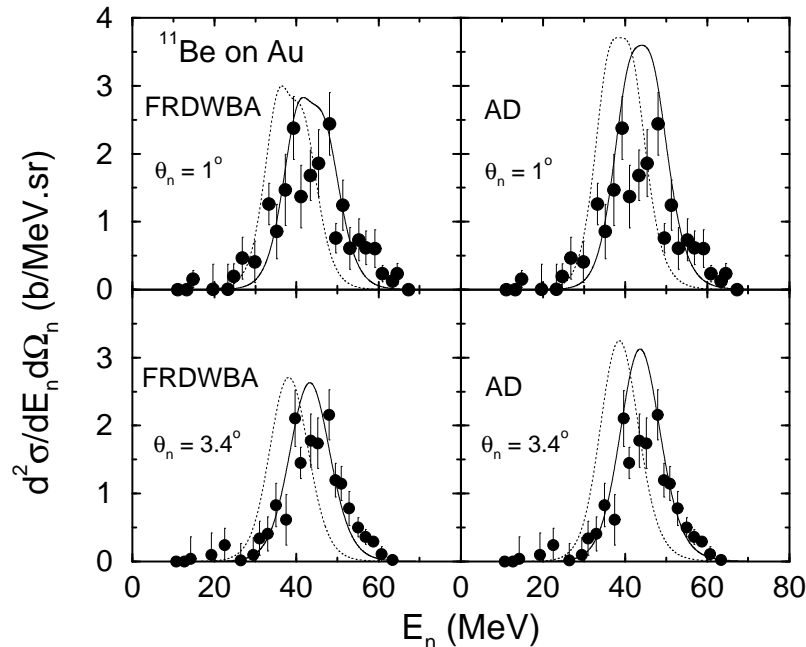


Fig. 3. Neutron energy distributions for the breakup of ^{11}Be on Au at beam energies of 37 MeV/nucleon (dotted lines) and 44 MeV/nucleon (solid lines), calculated using configuration (a) with single particle wave functions within the FRDWBA and the AD models. The top half of the figure is for $\theta_n = 1^\circ$, while the bottom half is for $\theta_n = 3.4^\circ$. The experimental data are taken from [28].

In Fig. 3, we present a comparison of our calculation with the data (taken from [28]) for the energy distribution of the neutron emitted in the same reaction as in Fig. 2 at two forward angles. Calculations performed within both FRDWBA and AD model are shown in this figure. The same configuration for the ^{11}Be ground state has been used in both the cases. The beam energy in this experiment [28] varies between 36.9 – 44.1 MeV/nucleon. To take into account this spread, we have performed calculations at both its upper (44 MeV/nucleon) (solid line) and lower ends (37 MeV/nucleon) (dotted line). Although these data have large statistical errors, the calculations performed at 44 MeV/nucleon are in better agreement with the experimental values. Thus our calculations may serve to remove the uncertainty in the data in this

regard. It should also be noted that the AD model calculations over-predict the experimental cross sections in the peak region.

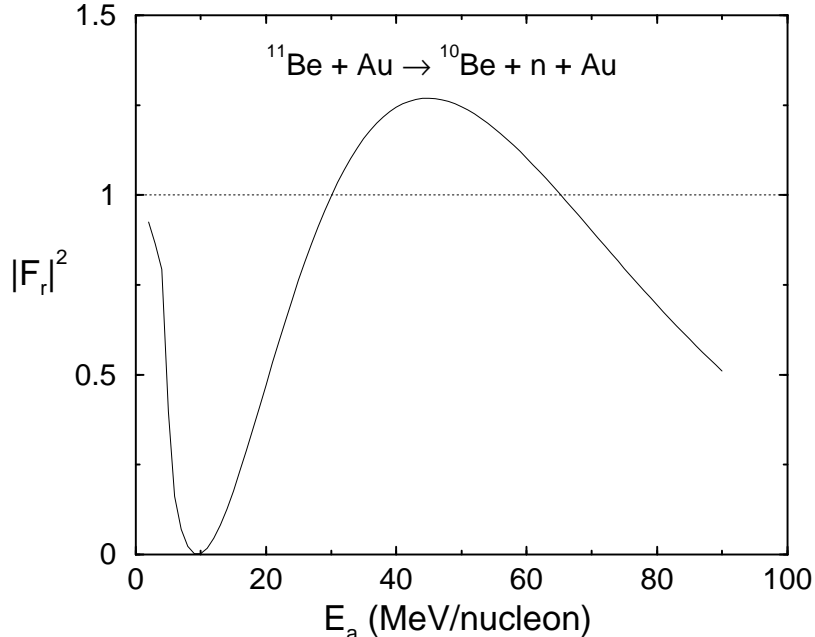


Fig. 4. Modulus square of the ratio F_r defined by Eq. (15) as a function of the beam energy for the same reaction as in Fig. 2 corresponding to forward emission angles of the breakup fragments as discussed in the text.

As discussed earlier, the cross sections obtained in the BT theory differs from that of the FRDWBA by the modulus square of the factor F_r as defined by Eq. (15). In fig. 4, we have shown the beam energy dependence of $|F_r|^2$ for the same reaction as in Fig. 2, for a set of forward angles of the outgoing fragments ($\theta_b = 1^\circ$, $\theta_c = 1^\circ$ and $\phi_c = 1^\circ$). We can see that this quantity is close to unity only at the sub-Coulomb beam energies (of course at higher beam energies it crosses twice the line representing the value 1). Therefore, the BT and FRDWBA calculations are expected to produce similar results at very low incident energies. Depending upon the beam energy, the BT results can be larger or smaller than those of the FRDWBA.

A comparison of the results of the FRDWBA (solid line) and the BT (dotted line) calculations for the same reaction as in Fig. 2 is presented in Fig. 5. The bombarding energy in this case is 44 MeV/nucleon. We can see that the BT results are larger than those of the FRDWBA in almost entire region of neutron energies. This is to be expected from the results shown in Fig. 4, where the quantity $|F_r|^2$ is larger than unity at this beam energy. It may be noted that the FRDWBA results provide a reasonable good description of the data, particularly in the peak region while BT calculations overestimate them.

In Fig. 6, we show the energy distributions of the charged fragment ^{10}Be , cal-

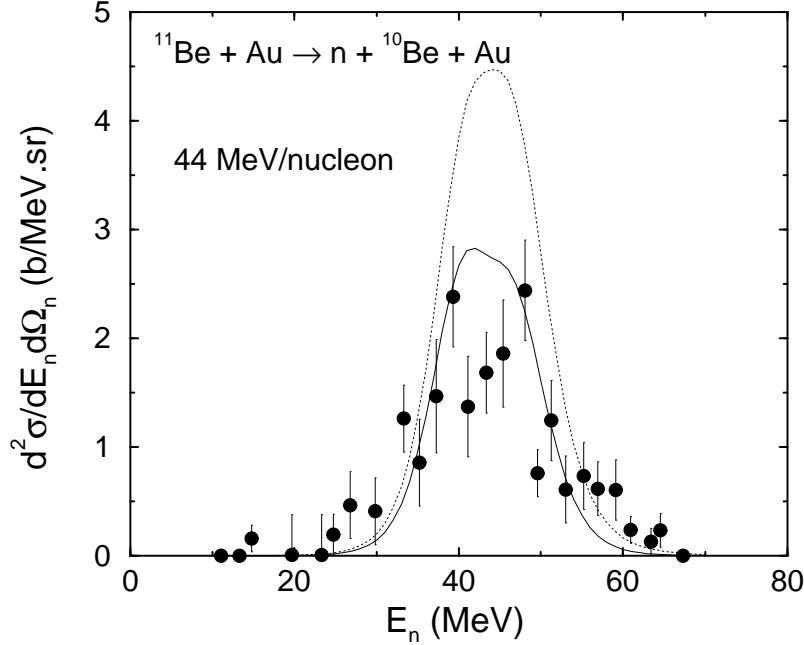


Fig. 5. The energy distribution of the neutrons observed in the breakup of ^{11}Be on the Au target at the beam energy of 44 MeV/nucleon at the neutron angle of 1° , calculated within the FRDWBA (solid line) and BT (dashed line) theories.

culated within the FRDWBA (upper part) and the AD model (lower part) for the breakup of ^{11}Be on the Au target at the beam energy of 42 MeV/nucleon at three angles of 1° , 2° and 3° . A noteworthy feature of these results is that the peak position in both the calculations is very close to the energy corresponding to the beam velocity. This suggests that the charged fragment gets almost no post acceleration in the final channel. This feature of the breakup of halo nuclei (which is in contrast to the case of the breakup of stable isotopes [30]), was first noted in Ref. [31], and was corroborated later on by the authors of Refs. [25,26,28,50]. The reason for not observing the post acceleration effects, as put forward by authors of Ref. [31], is that due to their very small binding energies the halo nuclei break up far away from the distance of closest approach, which reduces greatly the effect of Coulomb repulsion on the charged outgoing fragment. This argument has received support from a recent calculation of the Coulomb dissociation potential of the deuteron which is shown [51] to have a considerably large value even outside the charge density of the target nucleus. A separate reason for not observing this effect has been put forward by the authors of Ref. [28], according to which these effects are small as the collision time is much less than the characteristic time for the disintegration of the halo.

However, these quasiclassical arguments have been questioned by the authors of Ref. [27,52]. Esbensen, Bertsch and Bertulani [52], who include the higher order processes in the Coulomb dissociation of halo nuclei ^{11}Li and ^{11}Be by

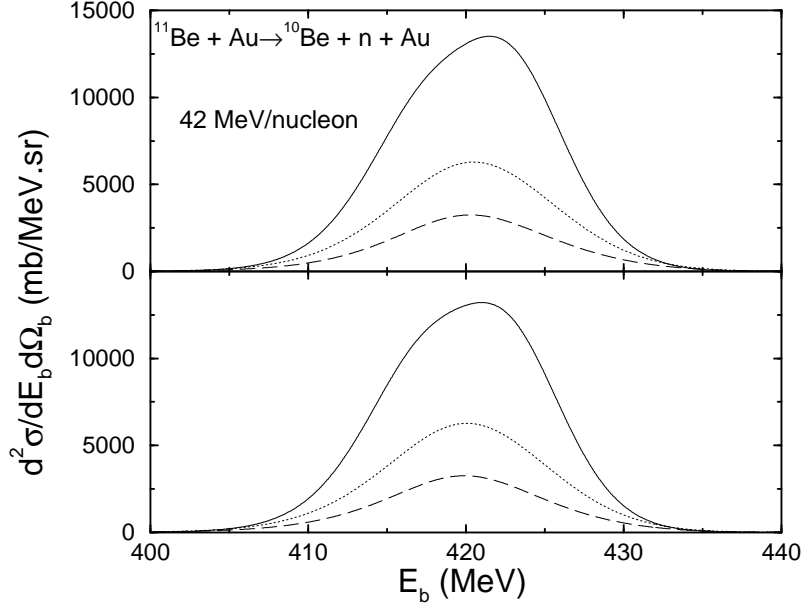


Fig. 6. Energy distribution of the ^{10}Be fragment in the breakup of ^{11}Be on Au at 42 MeV/nucleon beam energy corresponding to the ^{10}Be angles of 1° (solid line), 2° (dotted line) and 3° (dashed line). The FRDWBA and adiabatic model results are shown in the upper and lower parts of the figure respectively.

solving the three-dimensional time-dependent Schrödinger equation, and find a magnitude for the post acceleration effect which is quite appreciable for the ^9Li fragment in the breakup of ^{11}Li and relatively somewhat smaller for the ^{10}Be fragment in the breakup of ^{11}Be . In the semiclassical calculations of Baur, Bertulani and Kalassa [53], where breakup is assumed to take place at some classical distance, it is predicted that post acceleration effects should manifest itself in the increase of the average momentum of the charged fragment with the scattering angle. Indeed, the earlier measurements of Nakamura *et al.* [9] is consistent with this observation.

In a recent experiment [54], the momentum of the ^{10}Be core from the breakup of ^{11}Be has been measured with sufficient precision to verify the previously reported post acceleration effect. We have made a comparison of our FRDWBA calculations with this data in Fig. 7, where we show the calculated and experimental ^{10}Be average momenta (defined as $\sum p_b \frac{d^2\sigma}{dp_b d\Omega_b} / \sum \frac{d^2\sigma}{dp_b d\Omega_b}$) as a function of laboratory angle. In the semiclassical picture of Ref. [53], the impact parameter decreases with the increase of the scattering angle, thereby making the Coulomb repulsion effects on the charged fragment stronger. Therefore, the post acceleration should show up in the increase of this average momentum with the increase of the scattering angle. However, in both the experimental data of [54] as well as our calculations no such increase is observed. Thus, neither the data of Ref. [54] nor our calculations support the results found in Ref. [9]. Therefore, the semiclassical picture presented in [53] should be viewed

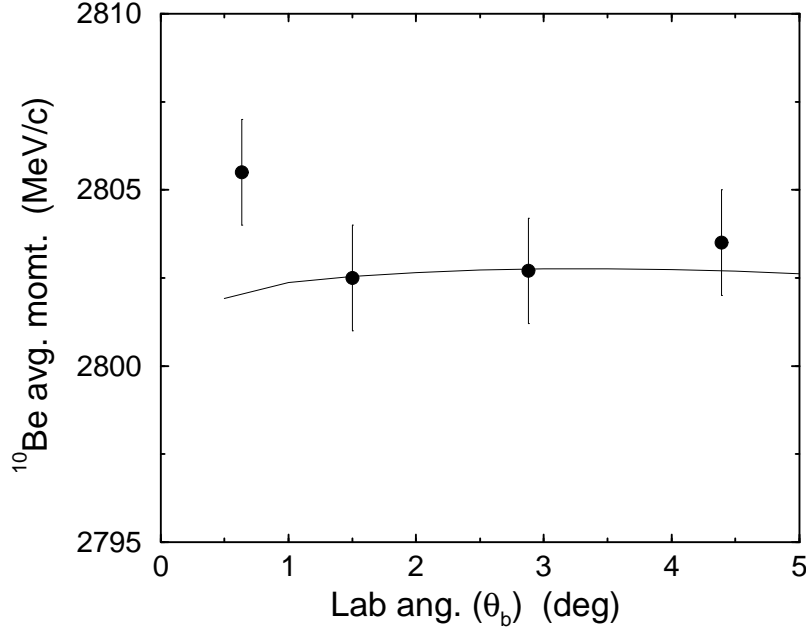


Fig. 7. Average momenta of the ^{10}Be fragment in the breakup of ^{11}Be on Au at 42 MeV/nucleon beam energy as a function of its detection angle. The data are taken from [54].

with caution.

3.1.2 Neutron Angular Distribution

The measured neutron angular distribution in the exclusive $^{11}\text{Be} + A \rightarrow ^{10}\text{Be} + n + A$ reaction below the grazing angle is very narrow and is shown to be [38,55] dominated by the Coulomb breakup process. This reflects the narrow width of the transverse momentum distribution of the valence neutron in the ground state of ^{11}Be , which is consistent with the presence of a neutron halo structure in ^{11}Be . In the top half of Fig. 8, we compare the calculated and measured exclusive neutron angular distribution $d\sigma/d\Omega_n$ as a function of the neutron angle θ_n for the above reaction on a Au target at the beam energy of 41 MeV/nucleon. Calculations (where integrations over the core fragment energy is done in the range of 390 to 430 MeV, which contributes most to the cross section) performed within the FRDWBA (solid line) and the AD model (dotted line) using the same configuration for the ^{11}Be ground state are shown in this figure. Also shown (dashed line) here is the FRDWBA calculation performed with the ^{11}Be ground state wave function obtained in the DCP model. We note that while the FRDWBA and the AD model results agree with each other well below 12° , the difference between the two models starts becoming prominent as the angle increases beyond this value, with the latter developing a dip around 25° . At small neutron angles, the FRDWBA calculation done with the DCP wave function overestimates somewhat the measured neutron

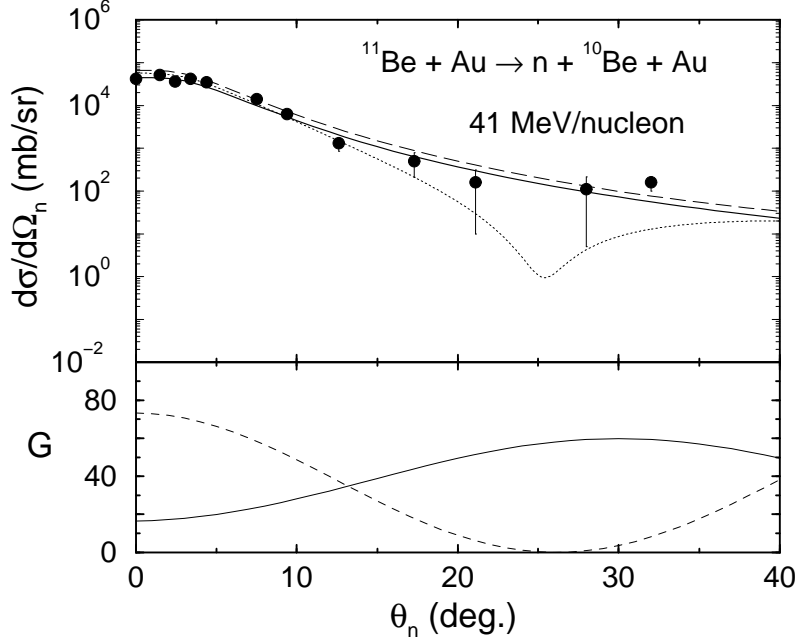


Fig. 8. The calculated neutron angular distributions for the breakup of ^{11}Be on a Au target at 41 MeV/nucleon beam energy (upper half). The solid and the dotted lines show the results of the calculation performed with the FRDWBA and AD model with configuration (a) using single particle wave functions, while the dashed line corresponds to the FRDWBA calculation done with the DCP wave function for the ground state of ^{11}Be as discussed in the text. The data are taken from [28]. In the lower half, the quantity G (see text) has been plotted against θ_n . The solid line and the dashed lines show the results for the FRDWBA and the AD cases respectively.

angular distribution.

To understand the origin of the dip in the AD model calculations of the neutron angular distribution, we have plotted the quantity $G(= \int d\theta_b \sin \theta_b |Z_\ell|^2)$ as a function of θ_n in the lower half of Fig. 8 for both the FRDWBA (solid line) and the AD (dashed line) cases. The energy of fragment b corresponds to the beam velocity. We can see that in the AD case G becomes very small around 25° , which corresponds to a node in its form factor at the momentum transfer related to this angle.

3.1.3 Relative energy spectrum of fragments

The relative energy spectrum for the breakup of ^{11}Be on a Pb target at 72 MeV/nucleon is shown in Fig. 9. The top half shows the results obtained with the FRDWBA (solid line) and the AD model (dotted line) using configuration (a) with the single particle wave function for the ^{11}Be ground state, while the bottom half depicts the FRDWBA results obtained with the single particle and DCP wave functions. We see that, while both the FRDWBA and the

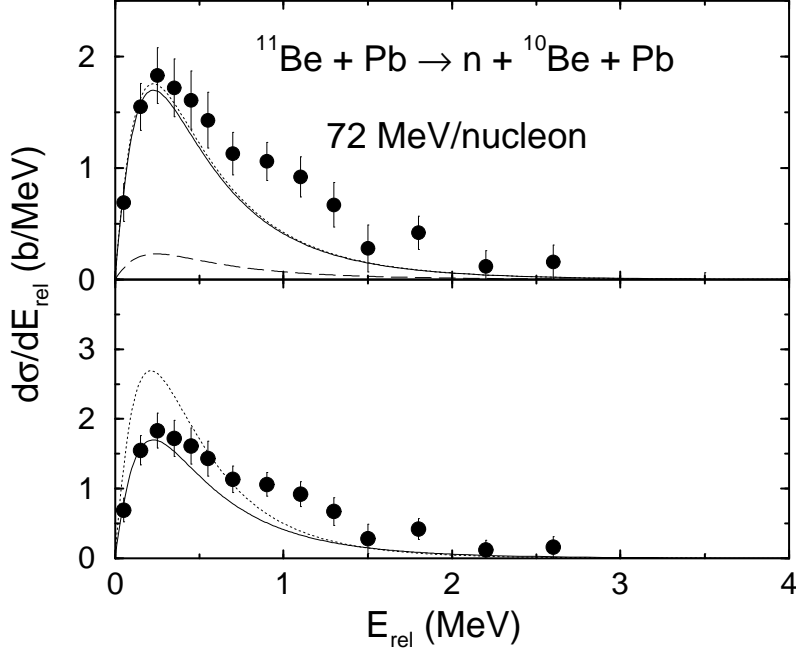


Fig. 9. Relative energy spectra for the Coulomb breakup of ^{11}Be on a Pb target at 72 MeV/nucleon beam energy. The top half of the figure shows the spectra obtained with a single particle wave function, using the FRDWBA (solid line), the AD model (dotted line) and the BT approximation (dashed line). The bottom half shows the results of FRDWBA calculations using single particle (solid line) and DCP (dotted line) wave functions. The data are taken from [9].

AD model calculations reproduce the peak value of the data [9] well, the FRDWBA calculations done with the DCP wave function overestimate it. On the other hand, none of the calculations is able to explain the data at higher relative energies. This can be attributed to the fact that nuclear breakup effects, which can contribute substantially [56] at higher relative energies (for $E_{rel} > 0.6$ MeV), are not included in these calculations. Of course, the authors of Ref. [9] claim that their data have been corrected for these contributions. However, the procedure adopted by them for this purpose is inadequate. They obtained the nuclear breakup contribution on the Pb target, by scaling the cross sections measured on a carbon target. This scaling procedure is unlikely to be accurate for reactions induced by halo nuclei due to the presence of a long tail in their ground state. In a full quantum mechanical theory, both Coulomb and nuclear breakup contributions should be calculated on the same footing and corresponding amplitudes should be added coherently to get the cross sections.

Calculations done using the BT theory (dashed line in the upper part of Fig. 9) underestimates the data considerably. This difference between the FRDWBA and the BT results can again be traced to the behavior of $|F_r|^2$ in Fig. 4, which is smaller than unity at the beam energy of 72 MeV/nucleon of this reaction.

We would like to remark that our post form FRDWBA results for the pure Coulomb breakup contribution to the relative energy spectra for the ^{11}Be agrees quite well with a recent calculation of the breakup reaction in a non-perturbative approach where the time evolution of the projectile is calculated by solving a time-dependent Schrödinger equation [57]. On the other hand, similar perturbative calculations performed previously [26] overestimate the data in the peak region.

3.1.4 Momentum distribution of the core

The neutron halo structure is reflected in the narrow width of the parallel momentum distribution (PMD) of the charged breakup fragments emitted in breakup reactions induced by the halo nuclei. This is because the PMD has been found to be least affected by the reaction mechanism [13–17] and therefore, a narrow PMD can be related to a long tail in the matter distribution in the coordinate space via Heisenberg’s uncertainty principle.

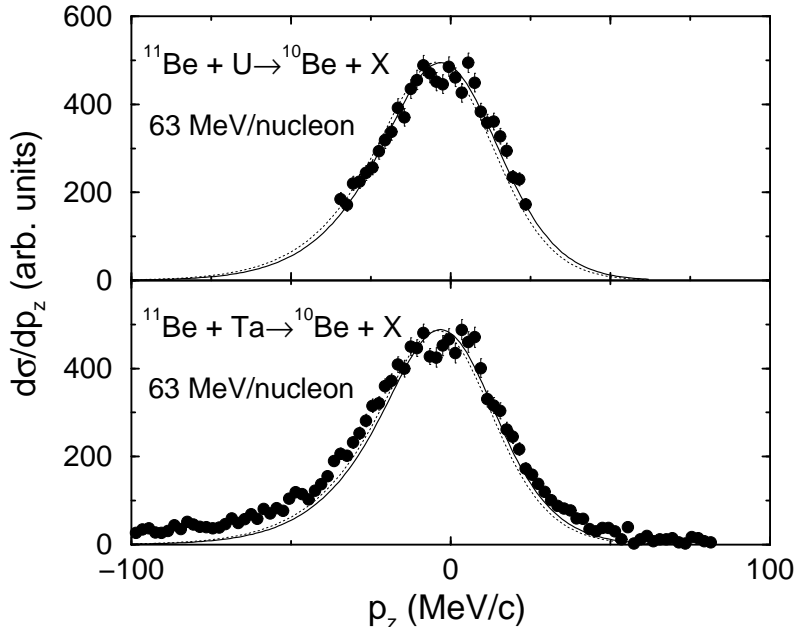


Fig. 10. Parallel momentum distributions of ^{10}Be in the breakup of ^{11}Be on U (top half) and Ta (bottom half) at 63 MeV/nucleon beam energy in the rest frame of the projectile. The same normalization has been used for both the FRDWBA (solid line) and the AD (dotted line) cases. The data are taken from [14].

In Fig. 10 we present the PMD of the ^{10}Be fragment emitted in the breakup of ^{11}Be on U and Ta targets at 63 MeV/nucleon beam energy. Calculations performed within both the FRDWBA and AD model formalisms using the configuration (a) are presented in this figure. The calculated cross sections are normalized to match the peak of the data points (which are given in arbitrary

units) [14], the normalization constant being the same for both cases. The full width at half maximum (FWHM) for the U and Ta targets are 44 MeV/c and 43 MeV/c respectively in both the FRDWBA and the AD cases. These agree well with the averaged experimental value of 43.6 ± 1.1 MeV/c [14] and also with those calculated in [38]. The very narrow widths of the parallel momentum distributions signal the presence of a neutron halo structure in ^{11}Be .

It may be noted that the calculations performed with configuration (c) gives results identical to that obtained with configuration (a). The PMD calculated with a pure d – wave configuration is too small in magnitude and too wide in width.

3.1.5 Coulomb part of total one-neutron removal cross section

For the breakup of ^{11}Be on a Au target at the beam energy of 41 MeV/nucleon, the values of the pure Coulomb total one-neutron removal cross section (σ_{-n}^C) are found to be 1.91 b and 1.94 b for the FRDWBA and the AD model respectively, using configuration (a) and the single particle wave function for the ground state of ^{11}Be . The corresponding values of σ_{-n}^C for the breakup of this projectile on the Pb target at the beam energy of 72 MeV/nucleon are 1.25 b and 1.29 barn respectively. The experimental values for the total one-neutron removal cross section (σ_{-n}) for these two reactions are reported to be 2.5 ± 0.5 b [28] and 1.8 ± 0.4 b [9] respectively. The difference between σ_{-n}^C and the experimental value of σ_{-n} can be attributed to the nuclear breakup effects. Incidentally, FRDWBA calculations performed with the DCP wave function for the ^{11}Be ground state leads to much larger values of 2.82 b and 1.76 b for σ_{-n}^C for the two cases respectively.

3.2 Results for $^{19,15,17}\text{C}$

In this section, we shall compare results of our calculations with the available data on the breakup of the neutron rich carbon nuclei $^{19,15,17}\text{C}$ on heavier targets.

There is a large uncertainty in the value of the last neutron separation energy in ^{19}C ($S_{n-18\text{C}}$) with quoted values varying between 160 – 530 keV [10,58]. It has recently been shown [59] that most of the available data on the Coulomb dissociation of ^{19}C can be satisfactorily explained within the adiabatic model of Coulomb breakup with the one-neutron separation energy of 530 keV. The ground state spin-parity of ^{19}C has been quoted as $1/2^+$, $3/2^+$ and $5/2^+$ [60]. The relativistic mean field (RMF) [61] as well as shell model calculations

Table 1

Searched depths of the Woods-Saxon potential for given projectile configurations and binding energies (ϵ) with radius and diffuseness parameters of 1.5 fm and 0.5 fm . The rms radius of the projectile is also shown for each case.

Projectile	Projectile configuration	ϵ (MeV)	V_{depth} (MeV)	Projectile rms radius (fm)
^{19}C	$^{18}C (0^+) \otimes 1s_{1/2}\nu$	0.530	49.77	3.19
	$^{18}C (0^+) \otimes 0d_{5/2}\nu$	0.530	53.58	2.95
	$^{18}C (0^+) \otimes 1s_{1/2}\nu$	0.160	47.43	3.66
^{15}C	$^{14}C (0^+) \otimes 1s_{1/2}\nu$	1.2181	61.21	2.83
	$^{14}C (0^+) \otimes 0d_{5/2}\nu$	1.2181	65.66	2.67
^{17}C	$^{16}C (0^+) \otimes 1s_{1/2}\nu$	0.729	54.45	3.03
	$^{16}C (0^+) \otimes 0d_{5/2}\nu$	0.729	58.70	2.81
	$^{16}C (2^+) \otimes 1s_{1/2}\nu$	2.5	62.55	2.79
	$^{16}C (2^+) \otimes 0d_{5/2}\nu$	2.5	60.82	2.86

using Warburton-Brown effective interaction [62] predict the spin-parity of the ground state of this nucleus to be $1/2^+$.

We use single particle wave functions which are constructed by assuming a Woods-Saxon interaction between the valence neutron and the charged core whose depth (for fixed values of the radius and diffuseness parameters) is adjusted to reproduce the binding energies of the nuclei under investigation. The valence neutron binding energies, searched potential depths (V_{depth}) and calculated rms radii of the projectile with different configurations for the ground state for each isotope are summarized in Table 1.

In this work, we consider two situations: (i) different binding energies (530 keV and 160 keV) with the same configuration for ^{19}C ground state ($^{18}C (0^+) \otimes 1s_{1/2}\nu$), and (ii) different configurations ($^{18}C (0^+) \otimes 1s_{1/2}\nu$ and $^{18}C (0^+) \otimes 0d_{5/2}\nu$) for ^{19}C ground state with the same binding energy (530 keV). We have considered single particle wave functions in all the cases, except for the 160 keV case where we have additionally considered a DCP wave function for the s – state [49]. It may be noted that for all the single particle wave functions, we have used a spectroscopic factor of 1.0.

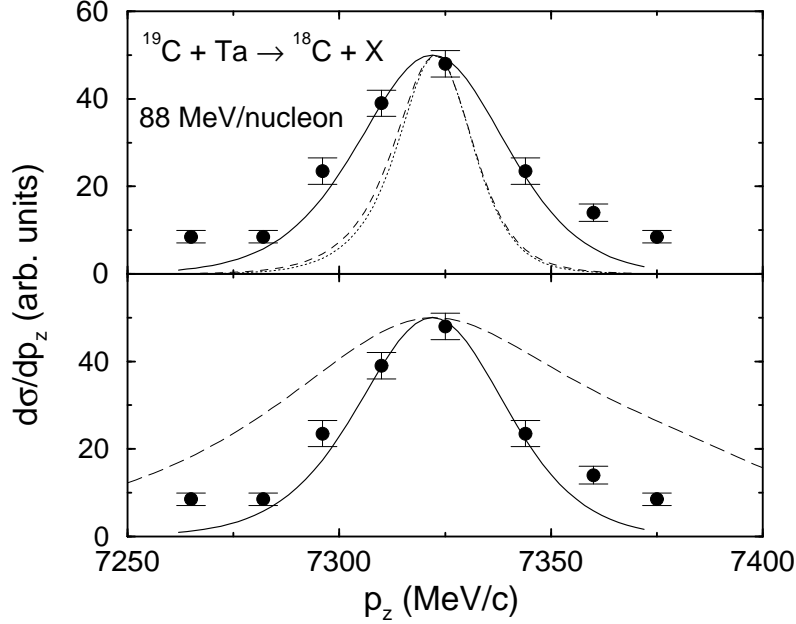


Fig. 11. FRDWBA results for the parallel momentum distribution of ^{18}C in the breakup of ^{19}C on Ta target at the beam energy of 88 MeV/nucleon. The top half shows the results obtained with the configuration ($^{18}\text{C}(0^+) \otimes 1s_{1/2}\nu$) and single particle wave function for the ground state of ^{19}C with one-neutron separation energies of 530 keV (solid line), 160 keV (dashed line). The dotted line shows the result obtained with a DCP wave function with a one-neutron separation energy of 160 keV. The bottom half shows the result obtained with the configurations ($^{18}\text{C}(0^+) \otimes 1s_{1/2}\nu$) (solid) and ($^{18}\text{C}(0^+) \otimes 0d_{5/2}\nu$) (dashed), with the same value of the one-neutron separation energy (530 keV). The data have been taken from [15].

In Fig. 11, we present the PMD (calculated within the FRDWBA formalism) of the ^{18}C fragment in the breakup of ^{19}C on a Ta target at the beam energy of 88 MeV/nucleon. We have normalized the peaks of the calculated PMDs to that of the data (given in arbitrary units) [15] (this also involves coinciding the position of maxima of the calculated and experimental PMDs). As can be seen from the upper part of this figure, the experimental data clearly favor $S_{n-^{18}\text{C}} = 0.53$ MeV with the s -wave n - ^{18}C relative motion in the ground state of ^{19}C . The results obtained with the s -wave configuration within the simple potential and DCP models (with the same value of $S_{n-^{18}\text{C}}$) are similar to each other.

In the lower part of Fig. 11, we have shown the results obtained with the d -wave relative motion for this system (with $S_{n-^{18}\text{C}} = 0.53$ MeV) and have compared it with that obtained with a s -wave relative motion with the same value of the binding energy. As can be seen, the FWHM of the experimental PMD is grossly over-estimated by the d -wave configuration. The calculated FWHM with the s -state configuration (with $S_{n-^{18}\text{C}} = 530$ keV) is 40 MeV/c, which is in excellent agreement with the experimental value of 41 ± 3 MeV/c

[15]. Thus these data favor a configuration $^{18}\text{C}(0^+) \otimes 1s_{1/2}$, with a one-neutron separation energy of 0.530 MeV for the ground state of ^{19}C . These results are in agreement with those of Ref. [59]. The narrow width of the PMD provides support to the presence of a one-neutron halo structure in ^{19}C .

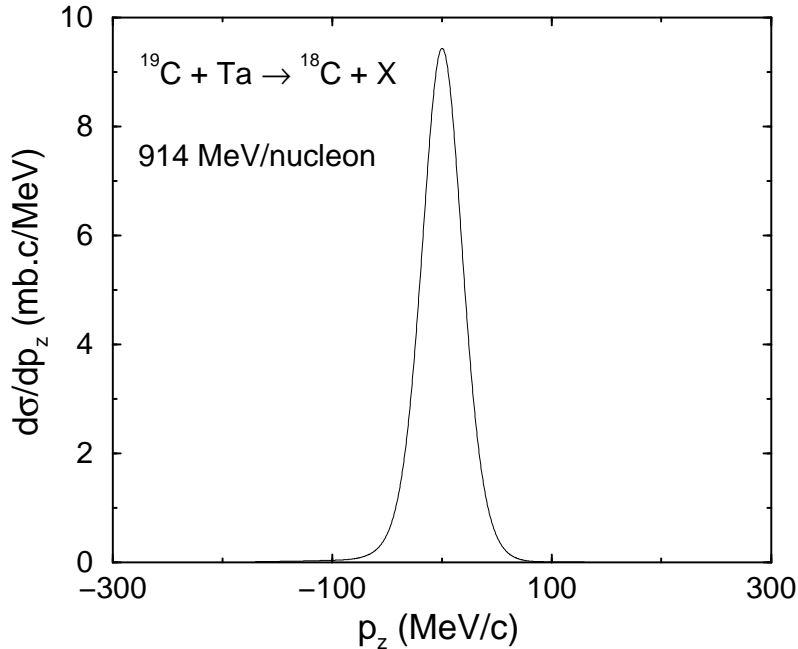


Fig. 12. Parallel momentum distribution of ^{18}C fragment in the Coulomb breakup of ^{19}C on Ta target at the beam energy of 914 MeV/nucleon.

The width of the PMD is not expected to change with beam energy [5]. To see this, we have calculated the PMD of ^{18}C in the Coulomb breakup of ^{19}C on a heavy target (Ta) at the high beam energy of 914 MeV/nucleon. The corresponding results are shown in Fig. 12. The FWHM of the distribution in this case is 42 MeV/c which is similar to that obtained above at a lower beam energy. However, FWHM of the PMD of the ^{18}C fragment measured in the breakup of ^{19}C on a carbon target at the same beam energy, has been found [18] to be of 69 ± 4 MeV/c. It would be interesting, therefore, to repeat measurement at this energy with a heavier target to check our observation.

In Fig. 13, we have shown the results of our FRDWBA calculations for the the relative energy spectrum for the breakup of ^{19}C on Pb at 67 MeV/nucleon beam energy. The experimental data is taken from [10]. The angular integration for the ^{19}C center of mass is done up to the grazing angle of 2.5° . It can be seen that in this case also the best agreement with the data (near the peak position) is obtained with the s - wave configuration with $S_{n-^{18}\text{C}} = 0.53$ MeV. Calculations done with the d - state configuration for both 530 keV and 160 keV one-neutron separation energy fails to reproduce the data. At the same time, those performed with the s - state configuration but with $S_{n-^{18}\text{C}} = 0.16$ MeV overestimates the data by at least an order of magnitude and

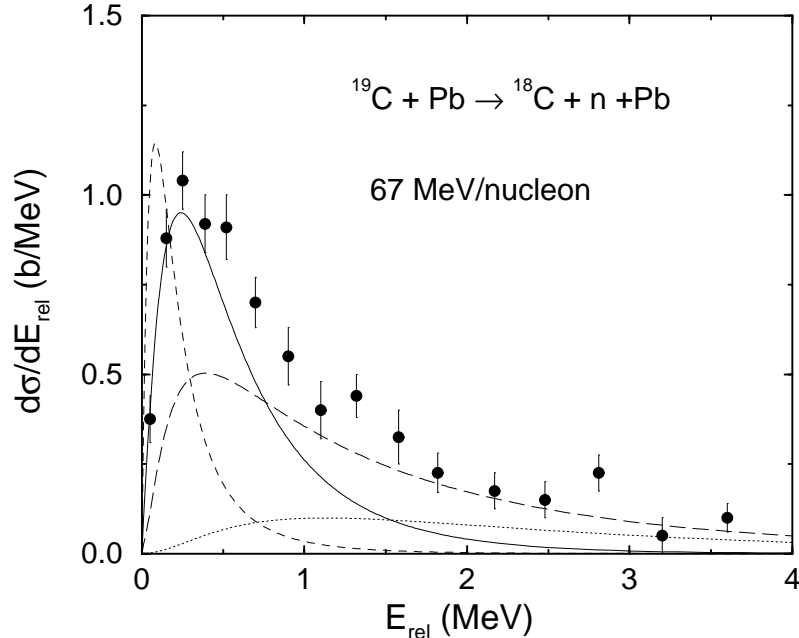


Fig. 13. Calculated relative energy spectra for the Coulomb breakup of ^{19}C on Pb at 67 MeV/nucleon. The d – state results, for binding energies 160 keV (long dashed) and 530 keV (dotted), are multiplied by 10. The 160 keV s – state result (short dashed) is multiplied by 0.086. The 530 keV s – state result is represented by the solid line. The data have been taken from [10].

also fail to reproduce the its peak position. However, as in the case of ^{11}Be , our calculations underestimate the relative energy spectrum for larger values of relative energies. In this case also, the proper consideration of the nuclear breakup effects is necessary to explain the data in this region. We would also like to remark that the correction for these effects made in the data [10] by scaling the cross sections for the breakup of ^{19}C on a carbon target is unlikely to be accurate due to the same reasons as stated in case of ^{11}Be .

Table 2 summarizes the FRDWBA results of σ_{-n}^C for the breakup of ^{19}C on different heavy targets at several beam energies. The experimental value of σ_{-n} for the breakup of ^{19}C on Ta at the beam energy of 88 MeV/nucleon is 1.1 ± 0.4 b [15]. It is seen from this table that only with the s – wave configuration of the ^{19}C ground state with $S_{n-^{18}\text{C}} = 0.53$ MeV, the calculated cross sections come closer to the experimental data. In this context it must be kept in mind that σ_{-n} also include contributions from the nuclear breakup effects, which is not included in our present calculations.

We next consider the breakup of ^{15}C which has a relatively larger value for the one-neutron separation energy (1.2181 MeV) and a ground state spin-parity of $1/2^+$ [15]. This can be obtained from two configurations: a $1s_{1/2}$ neutron coupled to a ^{14}C (0^+) core and a $0d_{5/2}$ neutron coupled to a ^{14}C (0^+) core. One could also considered a ^{14}C (2^+) core and $0d_{5/2}$ neutron coupling to get

Table 2

Calculated values of σ_{-n}^C for ^{19}C . ϵ is the one-neutron separation energy (MeV). The beam energy (E_{beam}) is in MeV/nucleon. The single particle wave functions are used in all the cases.

Projectile + target	ϵ	E_{beam}	SF	σ_{-n}^C (s -state) (mb)		σ_{-n}^C (d -state) (mb)	
				FRDWBA	AD	FRDWBA	AD
$^{19}\text{C} + \text{Ta}$	0.530	88	1	780.4	780.9	62.5	66.8
$^{19}\text{C} + \text{Ta}$	0.160	88	1	4029.4	4072.0		
$^{19}\text{C} + \text{Pb}$	0.530	67	1	744.96		25.7	
$^{19}\text{C} + \text{Pb}$	0.160	67	1	4246.0		84.9	

a $1/2^+$ ground state for ^{15}C , but it would raise the one-neutron separation energy to about 7.01 MeV, which is highly unfavorable for the formation of a halo. We, therefore, do not consider this configuration in our calculations.

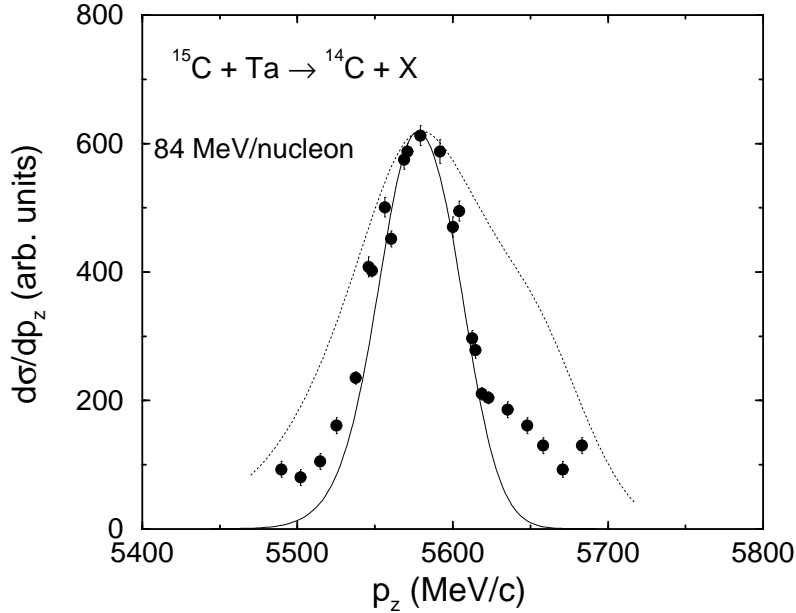


Fig. 14. Parallel momentum distributions of ^{14}C in the breakup of ^{15}C on Ta at 84 MeV/nucleon. The solid line and dotted lines show the results obtained with the configurations $^{14}\text{C} (0^+) \otimes 1s_{1/2}\nu$ the $^{14}\text{C} (0^+) \otimes 0d_{5/2}\nu$ respectively for the ground state of the projectile. The data have been taken from [15].

In Fig. 14, we present the results of our FRDWBA calculations for the PMD of the ^{14}C fragment in the breakup of ^{15}C on the Ta target at the beam energy of 84 MeV/nucleon. The experimental data is taken from [15]. As before, our calculations are normalized to the peak of the data. The s -state

Table 3

FWHMs from the parallel momentum distribution of ^{16}C for different ground state configurations of ^{17}C and one-neutron separation energies (ϵ) in the breakup of ^{17}C on Ta at 84 MeV/nucleon beam energy.

Projectile configuration	ϵ (MeV)	$FWHM$ (MeV/c)
$^{16}\text{C} (0^+) \otimes 1s_{1/2}\nu$	0.729	51
$^{16}\text{C} (0^+) \otimes 0d_{5/2}\nu$	0.729	114
$^{16}\text{C} (2^+) \otimes 1s_{1/2}\nu$	2.5	82
$^{16}\text{C} (2^+) \otimes 0d_{5/2}\nu$	2.5	185

configuration for the ground state of ^{15}C gives a FWHM of 62 MeV/c, while with the d – state configuration it comes out to be 140 MeV/c. Therefore, the experimental value for the FWHM (67 ± 1 MeV/c) [15] favors the former configuration. Hence our results provide support to the existence of a halo structure in ^{15}C . This nucleus provides an example of the one-halo system with the largest one-neutron separation energy, known so far.

^{17}C has a lower one-neutron separation energy (729 keV) as compared to that of ^{15}C . It would be interesting to see if it also has a halo structure, which seems probable if one considers only the binding energies. The quoted ground state spin-parities for this nucleus are $1/2^+$, $3/2^+$ and $5/2^+$ [60]. RMF calculations [61] predict it to have a value of $3/2^+$. We consider four possible ground state configurations for this nucleus and calculate the parallel momentum distributions of the ^{16}C fragment in the breakup of ^{17}C on a Ta target at 84 MeV/nucleon beam energy within our FRDWBA formalism. The FWHMs of the PMD obtained with different configurations are listed in Table 3.

It is evident from this table that the s – state configurations predict a narrow width for the PMD, providing support to the existence of a halo structure in this nucleus. The experimental data [15], however, is available only for the breakup of ^{17}C on a light target (Be) at 84 MeV/nucleon, which gives a FWHM of 145 ± 5 MeV/c. Since the PMD is mostly unaffected by the reaction mechanism [63], it is quite likely that the experimental FWHM will be the same also for the breakup of this nucleus on a heavier target. Therefore, the results shown in Table 3 seem to provide support to a d – wave configuration for the ground state of ^{17}C [64]. Hence, the existence of a one-neutron halo structure is quite improbable in ^{17}C . However, to arrive at a more definite conclusion in this regard the data on the breakup of ^{17}C on a heavy target is quite desirable.

4 Summary and conclusions

In this paper, we have performed calculations for the Coulomb breakup of the neutron rich nuclei ^{11}Be and $^{15,17,19}\text{C}$, which have a single valence neutron loosely bound with a stable core. We used a theory developed within the framework of the post form distorted wave Born approximation where finite range effects have been included approximately by using a local momentum approximation on the Coulomb distorted wave of the outgoing charged fragment. Within this method, the breakup amplitude is expressed as a product of factors describing separately the projectile structure and the dynamics of the reaction. This factored form of the breakup amplitude can also be obtained within an adiabatic model which makes the approximation that the strongly excited core-valence particle relative energies in the Coulomb breakup are small. However, unlike the post form DWBA, the adiabatic model does not use the weak coupling approximation to describe the center of mass motion of the fragments with respect to the target.

Both these theories allow the use of realistic wave functions for the ground state of the projectile. Furthermore, unlike the semiclassical and quantum mechanical theories using the zero range approximation which can be applied only to s – wave projectiles, these methods are applicable to projectiles with any relative orbital angular momentum structure between their fragments. This provides an opportunity to probe the structure of the ground state of the projectile, by comparing the predictions of these theories with the data for the breakup observable. We have calculated, the energy, angular and parallel momentum distributions of the fragments emitted in the breakup reaction of these nuclei using different configurations for their ground state, By making comparisons of the calculated cross sections with the available experimental data an effort has been made to put constraints on their ground state structure.

All the observable calculated by us are sensitive to the ground state configuration of the projectile. We find that for ^{11}Be , a s – wave configuration ($^{10}\text{Be}(0^+) \otimes 1s_{1/2}\nu$), with a spectroscopic factor of 0.74 for its ground state provides best agreement with the experimental data in all the cases. In our study, it is not possible to distinguish between this configuration and the one proposed recently where there is an admixture of the s – wave and a d – wave configuration, ($^{10}\text{Be}(2^+) \otimes 0d_{5/2}\nu$), with spectroscopic factors of 0.74 and 0.17 respectively for the ground state of this nucleus. For almost all the observables, there is a general agreement between the FRDWBA and adiabatic model results even in the absolute magnitude in the region where Coulomb breakup is expected to be dominant mode (ie. below the grazing angle). This provides additional support to our choice of the parameters associated with the local momentum in our FRDWBA calculations. It may be noted that the approximation of Baur and Trautmann, which also leads to the factored form for the

breakup amplitude, gives results which are very different from those obtained with the FRDWBA and AD model formalisms. The BT approximation fails to explain the data in most of the cases studied here.

In the case of neutron angular distributions for the breakup of ^{11}Be on the gold target at the beam energy of 41 MeV, there is a dip around 25° in the adiabatic model calculations, which is not seen in the corresponding FRDWBA results. It may be noted that this region was excluded in the results shown in Ref. [38]. This dip can be traced back to the fact that the form factor in the adiabatic model has a node at the momentum transfer corresponding to this angle. In any case, this region of the angular distribution is expected to get substantial contribution from the nuclear breakup effects (and also from the Coulomb-nuclear interference terms). Therefore, full implication of this dip can become clear only after nuclear breakup effects are included in these models.

For the ^{19}C case, the results for the PMD of ^{18}C and the relative energy spectrum of the $n + ^{18}\text{C}$ system show that the most probable ground state configuration of ^{19}C is $(^{18}\text{C}(0^+) \otimes 1s_{1/2}\nu)$ with a one-neutron separation energy of 530 keV and a spectroscopic factor of 1. Our FRDWBA calculations agree well with the experimental data of the MSU group [15]. By performing the calculations at GSI energies we note that the width of the PMD is independent of the beam energy. It would be interesting to perform the GSI experiment with a heavier target to check this prediction. Our FRDWBA results on ^{19}C are in excellent agreement with those of the adiabatic model [59].

We find that the most probable configuration for ^{15}C is a s – wave valence neutron coupled to the ^{14}C core and that for ^{17}C is a d – wave valence neutron coupled to a ^{16}C core. Both the experimental and the calculated FWHM of the PMD for the ^{14}C core in the breakup of ^{15}C are small and they agree well with each other. This provides support to the existence of a one-neutron halo structure in ^{15}C . On the other hand, in the case of ^{17}C the value of this quantity for the ^{16}C core is probably closer to that of a stable isotope. Therefore the existence of a halo structure in ^{17}C appears to be unlikely. Interestingly the one-neutron separation energies of ^{15}C and ^{17}C are 1.2181 and 0.729 MeV respectively. So the binding energy of the valence neutron as well as its configuration with respect to the core together decide whether a nucleus has halo properties or not.

5 ACKNOWLEDGMENTS

The authors are thankful to Horst Lenske for providing them the wave functions of the dynamical polarization model for various projectiles. One of the authors (RS) wishes to acknowledge several fruitful discussions with Dr. M.

A Validity of the local momentum approximation

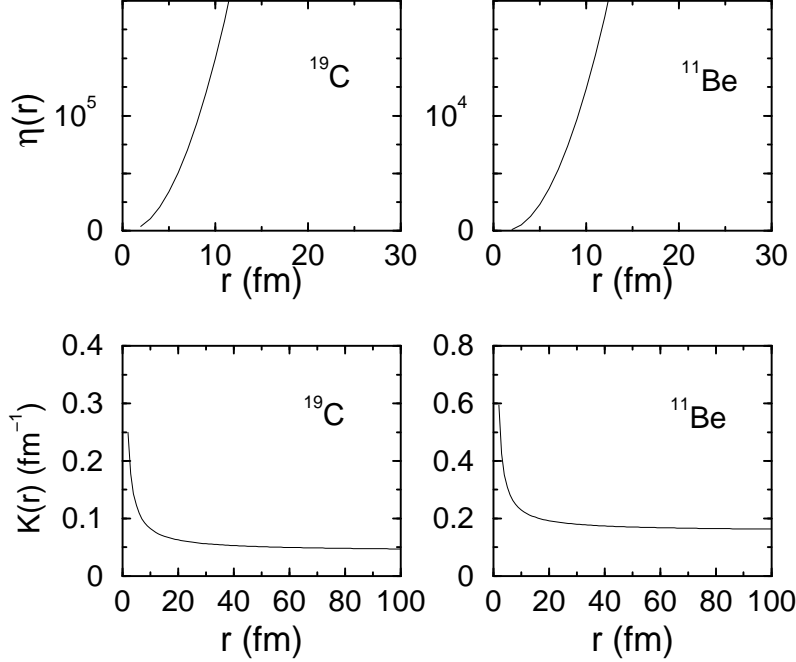


Fig. A.1. variation of $\eta(r)$ (upper half) and $K(r)$ (lower half) with r .

As discussed in [32], a condition for the validity of the local momentum approximation is that the quantity

$$\eta(r) = \frac{1}{2}K(r)|dK(r)/dr|^{-1} \quad (\text{A.1})$$

evaluated at a representative distance R should be much larger than R_{bc} , which is of the order of the range of the interaction V_{bc} . To check this, we show in Fig. A.1, $\eta(r)$ (upper half) and $K(r)$ (the magnitude of the local momentum) (lower half) as a function of r , for the breakup reactions $^{19}\text{C} + \text{Ta} \rightarrow ^{18}\text{C} + n + \text{Ta}$ at the beam energy of 88 MeV/nucleon (left side) and $^{11}\text{Be} + \text{Au} \rightarrow ^{10}\text{Be} + n + \text{Au}$ at the beam energy of 41 MeV/nucleon (right side). We see that for $r > 8 \text{ fm}$, $\eta(r)$ is several orders of magnitude larger than rms radii of the halo in both the cases. Therefore, the above condition is well satisfied.

From the lower half of Fig. A.1, we note that the value of $K(r)$ remains constant for distances larger than 10 fm. Due to the peripheral nature of the breakup reaction, this region contributes maximum to the cross section. Therefore, our choice of a constant magnitude for the local momentum evaluated at 10 fm is well justified. In fact, we noted that as R is increased from

5 to 10 fm the calculated cross sections vary by at the most 10%, and with a further increase the variation is less than 1%, in all the cases considered in this paper.

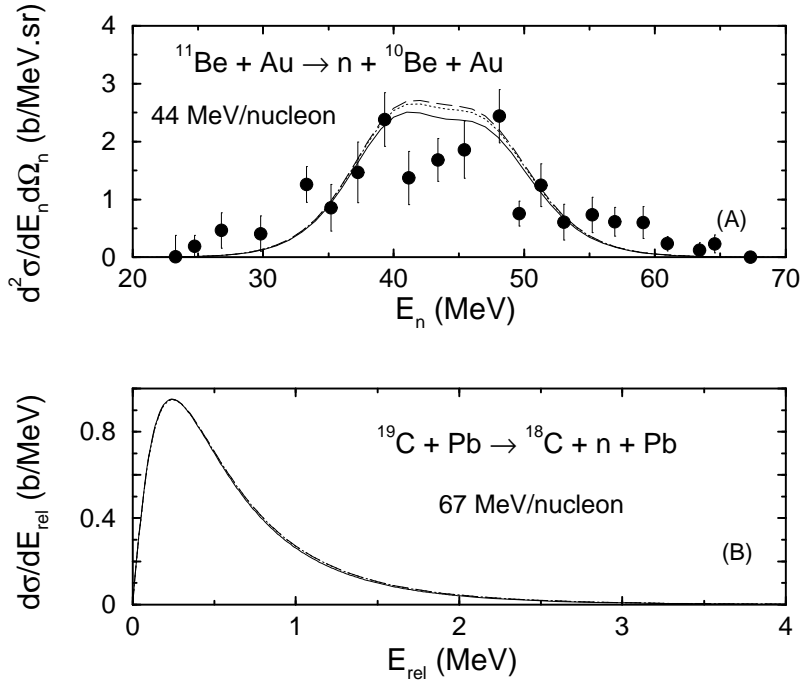


Fig. A.2. (A) The energy distributions of neutron from the breakup of ^{11}Be on Au at the beam energy of 41 MeV/nucleon and (B) relative energy spectra for the dissociation of ^{19}C on Pb at 67 MeV/nucleon for choices d_1 (solid line), d_2 (dashed line) and d_3 (dotted line) for the direction of the local momentum, as discussed in the text. For the relative energy spectra the results obtained in three cases are not distinguishable from each other.

In the application of the LMA in the description of the heavy ion induced transfer reactions, it was noted [35] that the calculated cross sections were more or less unaffected by the choice of the direction of the local momentum. However, in Ref. [38], some dependence of the breakup cross sections on this direction has been reported. To study the sensitivity of our FRDWBA results on the direction of \mathbf{K} , we have performed calculations for three cases where we take the angles of the local momentum (d_1) parallel to those of \mathbf{k}_b , (d_2) parallel to the direction corresponding to the half of the angles of \mathbf{k}_b and (d_3) parallel to the beam direction (zero angles).

In Table A.1, we show the results for σ_{-n}^C for the breakup of ^{11}Be and ^{19}C (on targets and at beam energies as indicated therein), for these three choices of the direction of \mathbf{K} . We see that between the cases d_1 to d_3 , the variation in the values of σ_{-n}^C is less than 5% for ^{11}Be , and less than 2% for ^{19}C . In part A of Fig. A.2, we show the energy distribution of the neutron for the same

Table A.1

Calculated value of the Coulomb part of one-neutron removal cross section for ^{11}Be for three different directions of local momentum (d_1) (d_2) and (d_3).

Projectile	ϵ	E_{beam}	SF	σ_{-n}^C	σ_{-n}^C	σ_{-n}^C
+ target	(MeV)	(MeV/nucleon)		d_1	d_2	d_3
				(mb)	(mb)	(mb)
$^{11}\text{Be} + \text{Au}$	0.504	41	0.74	1906	1973	1979
$^{19}\text{C} + \text{Pb}$	0.530	67	1	745	758	760

reaction as described in Fig. 2 The results obtained with cases d_1 , d_2 and d_3 are shown by solid, dashed and dotted lines respectively. We note that energy distributions calculated with these choices differ from each other only in the peak region; the variation between them is of the order of only 5%. The results for the neutron angular distribution (for the reaction reported in Fig. 8) is of the similar nature.

In part B of Fig. A.2, we show the relative energy spectrum for the same reaction as shown in Fig. (13), for the choices (d_1), (d_2) and (d_3). In this case we observe almost no variation in the calculated cross sections. Similarly, We have noted no dependence of the calculated widths of the parallel momentum distributions of heavy fragments on the direction of \mathbf{K} , in all the reactions investigated in this paper. Therefore, the dependence of various cross sections for the reaction studied in this paper, on the direction of the local momentum is either very minor or almost negligible. The measurements done so far are not able to distinguish the small differences that we see here in some cases. Therefore, we have performed all our calculations in this paper by using $\hat{\mathbf{K}} = \hat{\mathbf{k}}_b$.

References

- [1] I. Tanihata *et al.*, Phys. Rev. Lett. **55** (1985) 2676; Phys. Lett. B **160** (1985) 380; Phys. Lett. B **206** (1988) 592.
- [2] P. G. Hansen and B. Jonson, Europhys. Lett. **4** (1987) 409.
- [3] A. C. Mueller and B. M. Sherrill, Annu. Rev. Nucl. Part. Sci. **43** (1993) 591.
- [4] K. Riisager, Rev. Mod. Phys. **66** (1994) 1105.
- [5] P. G. Hansen, A. S. Jensen and B. Jonson, Annu. Rev. Nucl. Part. Sci. **45** (1995) 2.

- [6] I. Tanihata, J. Phys. G: Nucl. Part. Phys. **22** (1996) 157.
- [7] I. Tanihata *et al.*, Phys. Lett. B **206** (1988) 592; B. Blank *et al.*, Z. Phys. A **340** (1991) 41, M. Fukuda *et al.*, Phys. Lett. B **268** (1991) 339.
- [8] D. Sackett *et al.*, Phys. Rev. C **48** (1993) 118.
- [9] T. Nakamura *et al.*, Phys. Lett. B **331** (1994) 296.
- [10] T. Nakamura *et al.*, Phys. Rev. Lett. **83** (1999) 1112.
- [11] R. Anne *et al.*, Phys. Lett. B **250** (1990) 19; **304** (1990) 55.
- [12] F. M. Marqués *et al.*, Phys. Lett. B **381** (1996) 407.
- [13] N. A. Orr *et al.*, Phys. Rev. C **51** (1995) 3116.
- [14] J. H. Kelley *et al.*, Phys. Rev. Lett. **74** (1995) 30.
- [15] D. Bazin *et al.*, Phys. Rev. Lett. **74** (1995) 3569; Phys. Rev. **C57** (1998) 2156.
- [16] C.A. Bertulani and K.W. McVoy, Phys. Rev. C **46** (1992) 2638.
- [17] P. Banerjee and R. Shyam, Phys. Lett. B **349** (1995) 421.
- [18] T. Baumann *et al.*, Phys. Lett. B **439** (1998) 256.
- [19] C. A. Bertulani and G. Baur, Nucl. Phys. A **480** (1988) 615; M. S. Hussein, M. P. Pato and C. A. Bertulani, Phys. Rev. C **44** (1991) 2219.
- [20] G. F. Bertsch and H. Esbensen, Ann. Phys. (N.Y.) **209** (1991) 327; H. Esbensen and G. F. Bertsch, Nucl. Phys. A **542** (1992) 310.
- [21] R. Serber, Phys. Rev. **72** (1947) 1016.
- [22] F. Negoita *et al.*, Phys. Rev. C **54** (1996) 1787.
- [23] P. G. Hansen *et al.*, Phys. Rev. Lett. **77** (1996) 1016.
- [24] G. Baur and H. Rebel, J. Phys. G: Nucl. Part. Phys. **20** (1994) 1; Annu. Rev. Nucl. Part. Sci. **46** (1997) 321.
- [25] L. F. Canto, R. Donangelo, A. Romanelli and H. Schulz, Phys. Lett. B **318** (1993) 415; C. A. Bertulani, L. F. Canto and M. S. Hussein, Phys. Lett. B **353** (1995) 413.
- [26] T. Kido, K. Yabana and Y. Suzuki, Phys. Rev. C **50** (1994) R1276.; **53** (1996) 2296.
- [27] G. F. Bertsch and C. A. Bertulani, Nucl. Phys. A **556** (1993) 136; C. A. Bertulani and G. F. Bertsch, Phys. Rev. C **49** (1994) 2839; H. Esbensen, G. F. Bertsch and C. A. Bertulani, Nucl. Phys. A **581** (1995) 107.
- [28] R. Anne *et al.*, Nucl. Phys. A **575** (1994) 125.
- [29] C. A. Bertulani, G. Baur and M.S. Hussein, Nucl. Phys. A **526** (1991) 751.

- [30] G. Baur, F. Rösler, D. Trautmann and R. Shyam, *Phys. Rep.* **111** (1984) 333.
- [31] R. Shyam, P. Banerjee and G. Baur, *Nucl. Phys. A* **540** (1992) 341.
- [32] R. Shyam and M. A. Nagrajan, *Ann. Phys. (N.Y.)* **163** (1985) 285.
- [33] J. A. Tostevin, S. Rugmai and R. C. Johnson, *Phys. Rev. C* **57** (1998) 3225; J. A. Tostevin *et al.*, *Phys. Lett. B* **424** (1998) 219
- [34] P. Braun-Munzinger and H. L. Harney, *Nucl. Phys. A* **233** (1974) 381.
- [35] P. Braun-Munzinger, H.L. Harney and S. Wenneis, *Nucl. Phys. A* **236** (1974) 190.
- [36] G. R. Satchler, *Direct Nuclear Reactions*, Oxford University Press, New York, 1991.
- [37] G. Baur and D. Trautmann, *Nucl. Phys. A* **191** (1972) 321.
- [38] P. Banerjee, I. J. Thompson and J. A. Tostevin, *Phys. Rev. C* **58** (1998) 1042.
- [39] R. C. Johnson, J. S. Al-Khalili and J. A. Tostevin, *Phys. Rev. Lett.* **79** (1997) 2771.
- [40] J. A. Christley, J. S. Al-Khalili, J. A. Tostevin and R. C. Johnson, *Nucl. Phys. A* **624** (1997) 275.
- [41] R. C. Johnson, *J. Phys. G: Nucl. & Part. Phys.* **24** (1998) 1583.
- [42] H. Fuchs, *Nucl. Instrum. Methods* **200** (1982) 361; G. G. Ohlsen, *Nucl. Instrum. Methods* **37** (1965) 240.
- [43] A. Nordsieck, *Phys. Rev.* **93** (1954) 785.
- [44] F. M. Nunes, I. J. Thompson and R. C. Johnson, *Nucl. Phys. A* **596** (1996) 171.
- [45] D. L. Auton, *Nucl. Phys. A* **157** (1970) 305.
- [46] B. Zwieglinski, W. Benenson, and R. G. H. Robertson, *Nucl. Phys. A* **315** (1979) 124.
- [47] T. Aumann *et al.*, *Phys. Rev. Lett.* **84** (2000) 35.
- [48] J. S. Al-Khalili and J. A. Tostevin, *Phys. Rev. Lett.* **76** (1996) 3903.
- [49] H. Lenske, *J. Phys. G: Nucl. & Part. Phys.* **24** (1998) 1429, and private communication.
- [50] P. Banerjee, *Phys. Rev. C* **59** (1999) 2305.
- [51] A. Ingemarsson and R. Shyam, *Phys. Rev. C* **60** (1999) 054615.
- [52] H. Esbensen, G. F. Bertsch and C. A. Bertulani, *Nucl. Phys. A* **581** (1995) 107.

- [53] G. Baur, C. A. Bertulani and D. M. Kalassa, Nucl. Phys. A **550** (1992) 527.
- [54] J. E. Bush *et al.*, Phys. Rev. Lett. **81** (1998) 61.
- [55] P. Banerjee and R. Shyam, Phys. Lett. B **318** (1993) 268.
- [56] C. H. Dasso, S. M. Lenzi and A. Vitturi, Nucl. Phys. A **539** (1999) 59.
- [57] V. S. Melezhik and D. Baye, Phys. Rev. C **59** (1999) 3232.
- [58] G. Audi *et al.*, Nucl. Phys. A **624** (1997) 1.
- [59] P. Banerjee and R. Shyam, Phys. Rev. C **61** (2000) 047301.
- [60] D. Ridikas, M. H. Smedberg, J. S. Vaagen, and M. V. Zhukov, Europhys. Lett. **37**, 385 (1997); Nucl. Phys. A **628**, 363 (1998).
- [61] Z. Ren, Z. Y. Zhu, Y. H. Cai and G. Xu, Nucl. Phys. A **605** (1996) 75.
- [62] E. K. Warburton and B. A. Brown, Phys. Rev. C **46** (1992) 923.
- [63] P. Banerjee and R. Shyam, J. Phys. G: Nucl. & Part. Phys. **22** (1996) L79.
- [64] Angela Bonaccorso, Phys. Rev. C **60** (1999) 054604.